UC Irvine

Title

Global (50°S–50°N) distribution of water vapor observed by COSMIC GPS RO: Comparison with GPS radiosonde, NCEP, ERA-Interim, and JRA-25 reanalysis data sets

Authors

Kishore, P
Ratnam, M Venkat
Namboothiri, SP
et al.
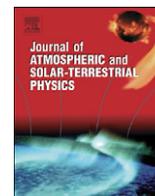
Global (50°S–50°N) distribution of water vapor observed by COSMIC GPS RO: Comparison with GPS radiosonde, NCEP, ERA-Interim, and JRA-25 reanalysis data sets

P. Kishore [a], M. Venkat Ratnam [b,*], S.P. Namboothiri [c], Isabella Velicogna [a], Ghouse Basha [b], J.H. Jiang [d], K. Igarashi [e], S.V.B. Rao [f], V. Sivakumar [g]

[a] Department of Earth System Science, University of California, Irvine, CA 92697, USA
[b] Department of Space, National Atmospheric Research Laboratory, Government of India, Tirupati, India
[c] School of Electrical and Electronics Engineering, SASTRA University, Tanjavur, India
[d] Jet Propulsion Laboratory, Pasadena, CA, USA
[e] Association of Radio Industries and Business (ARIB), Tokyo, Japan
[f] Deptartment of Physics, Sri Venkateswara University, Tirupati, India
[g] National Laser Centre, CSIR, Pretoria, South Africa

ARTICLE INFO

ABSTRACT

In this study, global (50°S–50°N) distribution of water vapor is investigated using COSMIC GPS RO measurements. Detailed comparisons have been made between COSMIC and high resolution GPS radiosonde measurements across 13 tropical stations and model outputs (ERA-Interim, NCEP, and JRA-25 reanalyses data sets). In comparison with independent techniques like radiosonde (Väisälä), it is found that COSMIC GPS RO wet profiles are accurate up to 7–8 km (assuming radiosonde as standard technique). In general, comparisons with corresponding seasonal means of model outputs are qualitatively in good agreement, although they differ quantitatively especially over convective regions of South America, Africa, and Indonesia. In tropical latitudes, the COSMIC specific humidity values are higher than the model outputs. Among various model outputs, ERA-Interim data set show near realistic features to that observed by COSMIC GPS RO measurements. Large asymmetry in the specific humidity distribution is observed between northern and southern hemispheres.

1. Introduction

Water vapor is the most important greenhouse gas in the Earth's atmosphere, inducing about two third of the natural greenhouse effect. As such, understanding the mechanisms that regulate it is of central importance for understanding past and future climate change. The lack of adequate data limits our ability to analyze or simulate important aspects of the global climate system (Ramanathan, 1981; Held and Soden, 2000). Currently, atmospheric water vapor measurements are made from a variety of sources including radiosondes, aircrafts and by various satellite instruments.

The radiosonde network is one of the reliable sources of the longest record of humidity in the troposphere and lower stratosphere. The radiosonde data have been the backbone for operational forecasting and a key data source for climate analysis.

Radiosonde observations have also been used as a benchmark to calibrate satellite remote sensing observations and validate satellite-retrieved soundings. Oort (1983) reported the first global distributions of specific humidity based on radiosonde data from 1963 to 1973 and made a detailed description of the vertical variability at 11 different vertical levels. Peixoto and Oort (1996) summarized the general features of the water vapor distribution using precipitable water vapor, specific humidity, and relative humidity based on the 10-year data sets. Globally, there are roughly 850 radiosonde stations using about fourteen types of radiosonde systems (Kuo et al., 2005). These measurements only cover limited area and even the distribution of radiosonde stations is rather inhomogeneous. Especially, the atmosphere over the oceans and a wide region in the southern hemisphere (SH) are not covered by these radiosondes. Hence these data sets need considerable care for the usage to drive any kind of long-term trends (e.g., Lanzante and Klein, 2003a; Lanzante et al., 2003b; Randel and Wu, 2006). Instrumental changes are a particular source of problems (Seidel et al., 2004), but can often be identified readily by sharp discontinuities in the record (Angell, 2003; Rosenlof and Reid, 2008). In addition, radiosondes

are known to suffer from radiation errors in temperature measurements and have a various errors/bias in humidity data (e.g., Luers and Eskridge, 1998; Wang et al., 2003). However, there are several factors like contamination from packing, errors in the calibration model at cold temperatures, ageing of the sensor, radiation bias due to solar heating of the sensor, etc., also affects the accuracy of radiosonde humidity measurements which are well reported (for example see Soden et al., 2004). Detailed discussion on the sources for biases in the radiosonde water vapor measurements is explained by Anna Agustí-Panareda et al. (2009).

There have been efforts to retrieve the global water vapor distribution from either infrared or microwave space-based observations (Prabhakara et al., 1982; Trenberth and Guillemot, 1995) and these measurements cover the radiosonde data gaps over the oceans, and even over some land areas. Most commonly used are microwave sensors which are able to provide water vapor distribution at a high spatial (horizontal) resolution (Bauer and Schlussel, 1993). By making measurements at different frequencies near 60 GHz, different atmospheric layers can be sampled. A series of nine instruments called Microwave Sounding Units (MSU) began to make such kind of measurements in late 1980s. Most of these measurements cover upper troposphere and lower stratosphere, with vertical resolution of ~ 2–3 km and spatial resolution of ~ 300–500 km and provide the global coverage within few days (2 or 3 days). However, MSU and advanced MSU (AMSU) data are influenced by instrument and orbit changes, calibration problems, instrument drifts, and insufficient vertical resolution (Anthes et al., 2000).

In recent years, radio occultation (RO) data using Global Navigation Satellite System (GNSS) signals emerged as powerful tool while overcoming problems of traditional data sources due to their encouraging combination of high accuracy and vertical resolution, long-term stability due to intrinsic self calibration, all weather capability and global coverage of obtaining atmospheric density, pressure, temperature and water vapor profiles in the troposphere and lower stratosphere. However, caution is also advised in using GPS RO data for water vapor measurements, which may also be affected by multi-path effects, non-spherical symmetry of the Earth's atmosphere, or uncertainties in the ancillary temperature fields used in the retrieval (Rocken et al., 1997).

In this paper, we present a new data set of global measurements of specific humidity (Q) in the troposphere from the COSMIC GPS RO. Though we mention global distribution we restrict our discussion to topical and mid-latitudes (50°S–50°N), unless we mention explicitly, due to more complexities in these data set over Polar latitudes. We use this data to better understand the variability of specific humidity in the troposphere on various temporal and spatial scales. We also compare the variability with National Centers for Environmental Prediction-Reanalysis (NCEP-reanalysis), the Japanese 25-year reanalysis (JRA-25), and ERA-Interim reanalysis (ERA) data sets.

2. Database

2.1. COSMIC GPS-RO data sets

GPS-based radio occultation (GPS-RO) technique is a relatively new remote sounding technique and it exploits the radio signals received onboard a Low Earth Orbiting (LEO) satellite from atmospheric limb sounding (Melbourne et al., 1994; Hocke 1997; Kursinski et al., 1997; Rocken et al., 1997; Wickert et al., 2001; Hajj et al., 2002). The GPS RO measurement has a vertical resolution ranging from ~ 400 m to ~ 1.4 km, which is much higher than that of any other satellite data (Kursinski et al., 1997). Six-satellite based Constellation Observing System for Meteorology Ionosphere and Climate (COSMIC) was successfully launched in mid-April

2006 (Anthes et al., 2008). Since 17 July 2006, COSMIC GPS-RO has been providing accurate and high vertical resolution profiles of atmospheric parameters, particularly unaffected by clouds, precipitation or aerosols, and they are almost uniformly distributed over the globe. A distinctive feature of the COSMIC mission, compared to previous RO missions, is tracking both set and rise neutral atmospheric occultations in the lower troposphere in an open-loop (OL) mode (Schreiner et al., 2007). The open-loop tracking technique will significantly reduce the GPS RO inversion biases by eliminating tracking errors (Sokolovskiy et al., 2006). This is very important for detecting the moisture variation in the lower troposphere, which is very important for weather prediction and climate analysis. The retrieval of atmospheric profiles from GPS RO measurements has been described in detail by a number of authors (e.g., Melbourne et al., 1994; Kursinski et al., 1997; Kursinski and Hajj, 2001; Wickert et al., 2004). In the present study, we use the COSMIC RO data collected during the period from September 2006 to December 2009 analyzed by CDAC data center.

2.2. JRA-25 data sets

Since reanalysis data sets are used in many operational purposes, we have tested how good these data represents the true behavior of water vapor across the globe. For each RO profile a coinciding profile was extracted from the model data sets (ERA-Interim, NCEP, and JRA-25) i.e., spatially interpolated to the locations of the RO data using the nearest time. This approach ensures that potential sampling errors due to non-uniform distribution or limited coverage of RO observations by not perturbing the statistics.

A long-term global atmospheric reanalysis, named Japanese 25-year reanalysis (JRA-25) data sets was produced by the Japan Meteorological Agency (JMA) numerical assimilation and forecast system (Onogi et al., 2007). JMA's latest numerical assimilation system, and specially collected observational data, were used to generate a consistent and high-quality reanalysis data set designed for climate research and operational monitoring and forecasts. JRA-25 has a spectral resolution of T106 (equivalent to a horizontal grid size of around 120 km) and extends from the surface to about 50 km in the vertical. The analysis covers the period from 1979 to present. JRA-25 is available on 23 standard pressure levels spanning 1000–0.4 hPa with a horizontal resolution in longitude and latitude of $1.25° \times 1.25°$ and a time resolution of 6 h. The model assimilation has been described in detail in Onogi et al. (2007).

2.3. NCEP reanalysis data sets

The NCEP reanalysis uses a global numerical weather analysis/forecast system to perform data assimilation using historical observations (Kalnay et al., 1996; Kistler et al., 2001). These analyses are referred to as NCEP. These data are available on a $2.5° \times 2.5°$ grid on 17 pressure levels from 1000 to 10 hPa, from 1948 to present. The atmospheric variables, partially defined by the observations since the analysis incorporates rawinsondes, balloons, aircrafts, ships, surface stations, and satellites, were put through a quality check, fed into an assimilation model that includes parameterizations for all major physical processes, and finally examined again for self consistency.

2.4. ERA-interim data sets

Another database used in for present study is the operational analyses of the European Center for Medium-Range Weather Forecasts (ECMWF) global assimilation scheme. This model is one of most advanced in operational use and capable of predicting the global atmosphere with accuracy just barely less than what is theoretically possible (Simmons and Hollingsworth, 2002). We have

used a later and further improved version of the ECMWF model i.e., is ERA-Interim reanalysis. The selected variables are specific humidity, along with the temperature, zonal and meridional wind components on pressure levels. The atmospheric data are available on a $1.5° \times 1.5°$ grid on 37 pressure levels from 1000 to 1 hPa. ECMWF uses a 4D-var system based on a spectral GCM (e.g. Simmons et al., 2005). The main advances of the ERA-Interim reanalysis data assimilation over the ERA-40 system are: 6 hourly four dimensional variational analysis (4D-var), T255 horizontal resolution, better formulation of background error constraint, new humidity analysis, improved model physics, quality control of data drawing on experience from ERA-40, variational bias correction of satellite radiance data, improvements in radiosonde temperature, and surface pressure bias handling, more extensive uses of radiances (Simmons et al., 2007b; Uppala et al., 2008; Dee and Uppala, 2009).

3. Results and discussion

3.1. Comparison of specific humidity between COSMIC and GPS radiosonde data

Before going into the details of the specific humidity profiles observed by the COSMIC satellite, it is desirable to compare the observed specific humidity profiles with in-situ measurements. It is worth to mention here is that humidity profiles from GPS RO are retrieved using 1D-var technique (Poli et al., 2002). Note that 1D-var method is an effective way to combine information provided by GPS RO and a given priori atmospheric state in a statistically optimal way. As mentioned earlier, we use the COSMIC data analyzed by CDAC data center. We mainly focus on the tropical latitudes as much of the variability is noticed in these

regions. For this, we have selected 13 radiosonde stations distributed across the globe in the tropical latitudes where high resolution GPS radiosondes were launched. Location and names of these stations are presented in Fig. 1(a). Fig. 1(b) depicts a typical example showing comparison of specific humidity between COS-MIC and Singapore (1.37°N, 103.98°E) radiosonde observed on 05 September 2006 at 12 UT. COSMIC specific humidity profile refers to 0.24°N, 102.28°E observed at 13 UT which corresponds to the nearest pass from Singapore. The specific humidity is derived from the water vapor and pressure using the method given by Ross and Elliott (1996). One can see a very good correlation between the two independent techniques both in the trend and magnitude above about 1.5 km. Fig. 1(c) shows the statistical mean difference of specific humidity between radiosonde and COSMIC for 78 cases of Singapore. We have selected profiles from COSMIC which are within $\pm 2°$ latitude and longitude difference and 2 h time difference in order to make realistic correlations between the two. Note that large differences of nearly 2 g/kg occur below 1.5 km and a good correlation can be noticed above. In order to represent more meaningful comparison we have shown the fractional mean difference (radiosonde-COSMIC/COSMIC) between the two in Fig. 1(d). This fractional difference is negative (positive) in higher (lower) altitudes and above 7 km very large difference is observed. Number of profiles reaching down to surface from COSMIC is very low which is shown at the top axis (Fig. 1d) and this could be one of the reasons for large difference below 1.5 km. Dry bias in lower troposphere may be because of radiosondes are point measurements where as COSMIC are having horizontal resolution of about ∼100 km (Ho et al., 2010) in addition to the biases discussed extensively by earlier authors (Ao et al., 2003; Beyerle et al., 2004).

A good correlation (∼0.8) can be noticed up to the altitude of 8 km between the two suggesting that COSMIC specific humidity profiles are reliable up to 8 km (assuming radiosonde as a standard
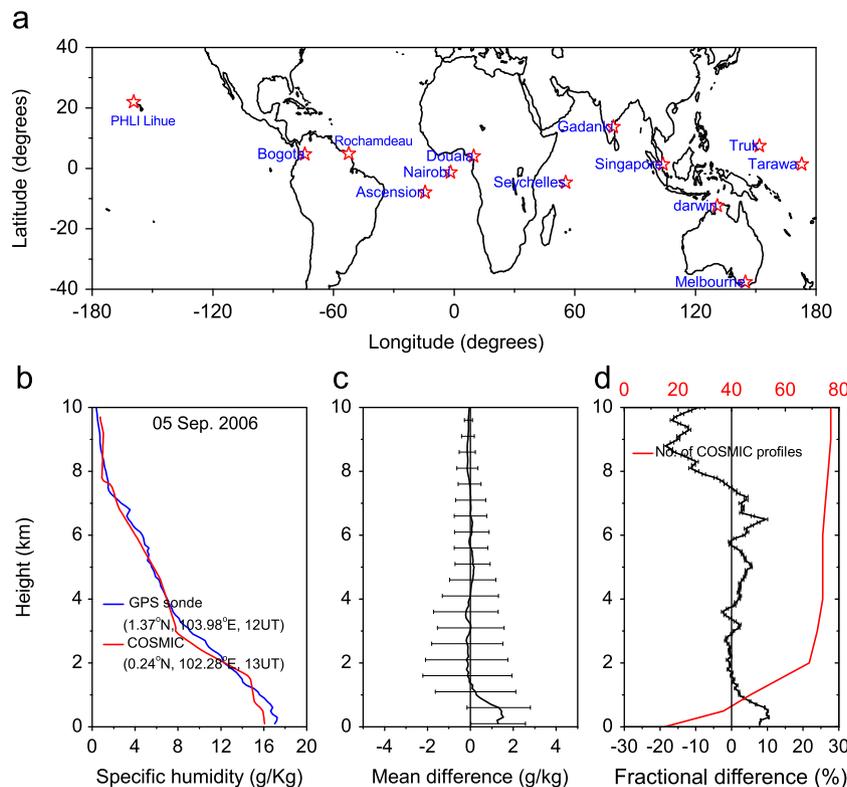

Fig. 1. (a) Map showing the locations and names of the radiosonde stations chosen for comparing water vapor measured with COSMIC. (b) Typical example showing the comparison of specific humidity between Singapore radiosonde and nearby overpass of COSMIC. (c) Mean and (d) fractional difference in specific humidity between Singapore radiosonde and COSMIC for 78 cases. Horizontal bars are standard deviations. Red line (d) represents the number of profiles reaching down to surface from COSMIC. (For interpretation of the references to color in this figure legend, the reader is referred to the web version of this article.)

technique). Here it is worth to mention that while deriving COSMIC humidity profile, these radiosonde data sets might have already gone into 1D-var retrieval technique as an initial point (Poli et al., 2002). This could be one of the reasons for high correlations observed in the present case. However, we have checked further with the Gadanki (13.5°N, 79.2°E) radiosonde data (Rao et al., 2009) which have not gone into the forecast and found similar correlations. Table 1 shows the mean difference in the specific humidity (g/kg) and standard deviation observed at various altitudes from all the stations mentioned in Fig. 1(a) for both 00 and 12 UT separately. Number of profiles selected for comparing with COSMIC is also provided in the brackets. Note that the profiles reaching down to 1.4 km are only used for this table. Less standard deviation is noticed from the table at higher altitudes. Less number of profiles reaching down to surface in case of COSMIC could be the one of the reasons for the observed differences between radiosonde and COSMIC besides the large spatial

selection (±2° latitude and longitude) considered for the comparison. However, a limited number of co-incidences or the spatial selection criterion may not explain completely a large bias without further effects coming into play which needs further investigations.

Nevertheless, very good correlations are observed up to 7–8 km from the mean profiles (figures not shown), suggesting that COSMIC profiles are of high precision up to this altitude. Note that correlations are higher at 12 UT than 00 UT. A consistent positive bias is noticed at the all altitudes between radiosonde and GPS RO data sets at both the times which need further investigations to explore possible reason for the same.

3.2. Longitudinal–latitudinal variability of the specific humidity

In this sub-section, we describe the global structures of the specific humidity derived from COSMIC RO measurements and

Table 1
Mean specific humidity (g/kg) observed by GPS radisondes at various altitudes obtained from all the stations mentioned in Fig. 1(a) for both 00 and 12 UT separately. Mean difference and standard deviations observed between radiosondes and COSMIC along with correlation coefficients are also provided. Number of profiles selected for comparing (see text for selection criteria) with COSMIC is also provided in the brackets. Note that the profiles reaching down to 1.4 km are only used for this table.

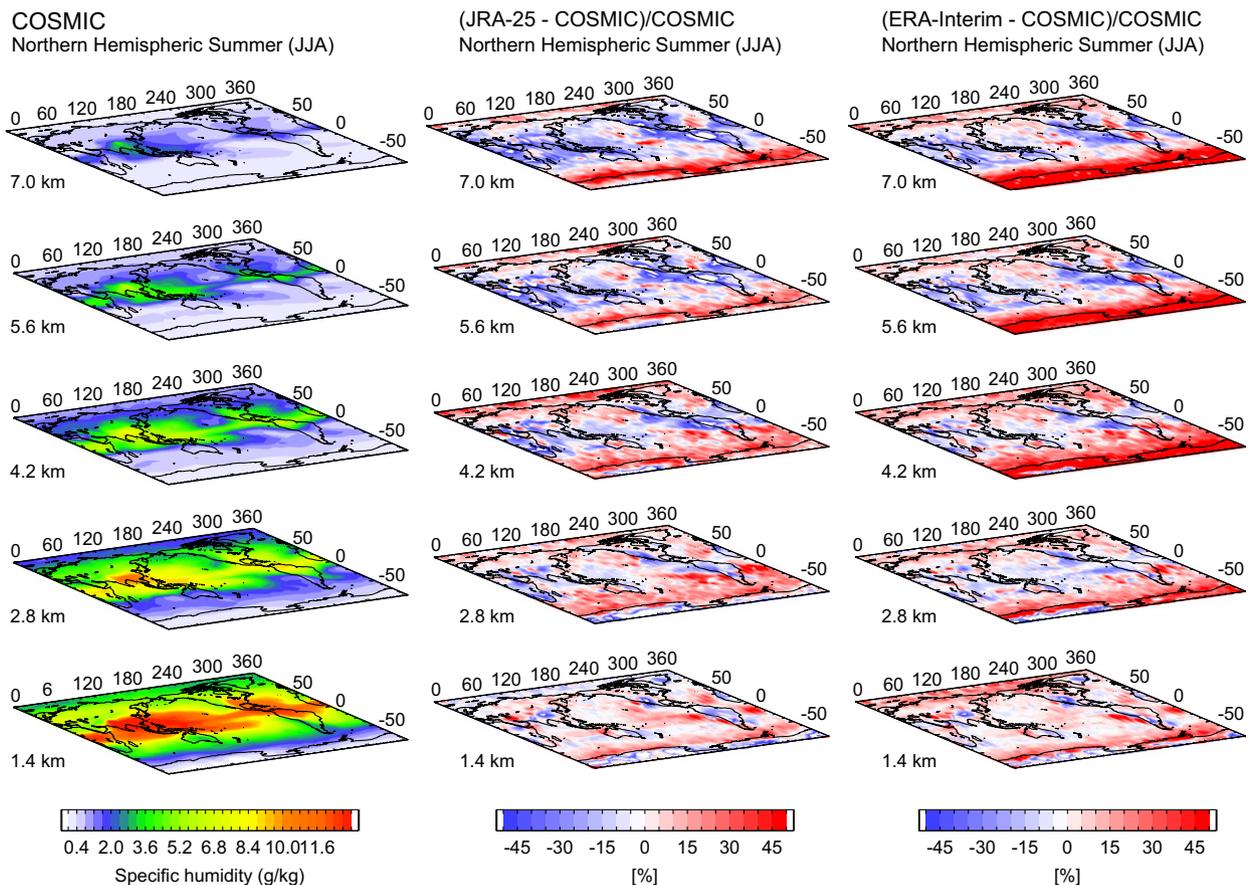| Altitude (km)	00 UT (365)			12 UT (757)		
	Radiosonde mean	Mean diff. ± SD	Correlation	Radiosonde mean	Mean diff. ± SD	Correlation
1.4	13.54	4.04 ± 2.92	0.78	13.72	4.22 ± 2.63	0.82
2.8	10.24	2.50 ± 2.97	0.80	9.64	1.99 ± 2.65	0.85
4.2	5.15	1.85 ± 2.18	0.80	4.83	1.53 ± 2.03	0.87
5.6	2.94	1.09 ± 1.74	0.74	2.99	1.06 ± 1.52	0.85
7.0	1.50	0.60 ± 0.99	0.79	1.72	0.68 ± 1.14	0.77

Fig. 2. Mean global specific humidity distribution observed by COSMIC during NH Summer (JJA) at different altitude levels averaged during 2006–2009. Relative mean difference observed in specific humidity globally between JRA-25 and COSMIC (JRA-25–COSMIC/COSMIC) (middle), and between ERA-Interim and COSMIC (ERA-Interim–COSMIC/COSMIC) (right) during same period at different altitude levels. (For interpretation of the references to color in this figure, the reader is referred to the web version of this article.)

compare with the model data sets during northern hemisphere (NH) summer (June, July, and August) and NH winter months (December, January and February) which are shown in Figs. 2 and 3 (left panels), respectively. Since the vertical resolution of GPS RO is about 1.5 km which is also close to reanalysis data set vertical resolution, we show the specific humidity at five altitude levels with resolution of 1.5 km starting at 1.4 km. Note that number of occultations reaching down to surface is small hence we have selected lower altitude as 1.4 km. The data used in this study have been gridded onto a $5° \times 5°$ longitude–latitude grid. From the Figs. 2 and 3, in general, enhanced values of specific humidity over the region of $30°S–30°N$ during summer and winter and decreasing with increasing altitude level can be noticed. The basic features present in COSMIC are very similar to those observed from reanalysis data sets (mean specific humidity distribution is not shown for reanalysis data sets). Most notable is the contrasting dry and moist regions over the tropics, reflecting the upward and downward branches of the Hadley cell, the zonal symmetry in the tropical Pacific indicative of the Walker circulation, and the moist areas associated with the mid-latitude storm tracks. First describing the NH summer season (Fig. 2a) particularly, it is interesting to note that the maximum values of specific humidity are over the north-eastern part of India and it extends up to the Pacific Ocean. The local maxima are seen also over the African and South American tropical regions. The highest values of specific humidity occur in the equatorial zone where the mean water vapor content of the air and the temperature are high. In this zone, the tropical convective systems connected with the inter-tropical convergence zone (ITCZ) dominate the circulation with a strong vertical transport and diffusion of water vapor associated with the ascending branch of the Hadley cell leading to the high specific humidity

(Peixoto and Oort, 1996). There is a distinct region of high water vapor located over north-eastern part of India in NH summer, which is caused by strong tropospheric convection linked with the Indian summer Monsoon. The largest seasonally averaged specific humidity values at 1.4 km are found in the vicinity of the south Asian/Indian monsoon ($15°N–20°N$ latitude and $70°–100°E$ longitude) during June to August months.

The specific humidity presented in Fig. 3(a) for the NH winter season exhibits large values over the North-east Asia, Malaysia, and Indonesia at 1.4 and 2.8 km altitude levels. Other two regions with enhanced specific humidity are over the Northern part of South America (especially Amazon region) and the Southern part of Africa. In the eastern tropical Pacific region, the area of increased specific humidity at all levels extends from approximately $5°N–25°S$ and $90°E–225°E$. During NH summer, Indian and the nearby East Asian regions exhibit comparatively larger intensities than NH winter season. Gettelman et al. (2006) reported high humidity values in deep layers over the tropical convective regions of South America, Africa, and the Western Pacific regions by the Atmospheric Infrared Sounder (AIRS).

The high specific humidity band associated with ITCZ migrates between southward position in NH winter and northward position in NH summer. In January the eastern equatorial Pacific is relatively dry, and hence the high-specific humidity band breaks over this region. The tropical high specific humidity extends far northward into eastern Asia and North pacific, and the south-eastern United States and the western Atlantic. In the extra tropics of the SH the specific humidity reaches the highest values in January and the lowest in July. Similarly, specific humidity in the NH extra-tropics has its peak in the northern summer and its lowest values in the northern winter.
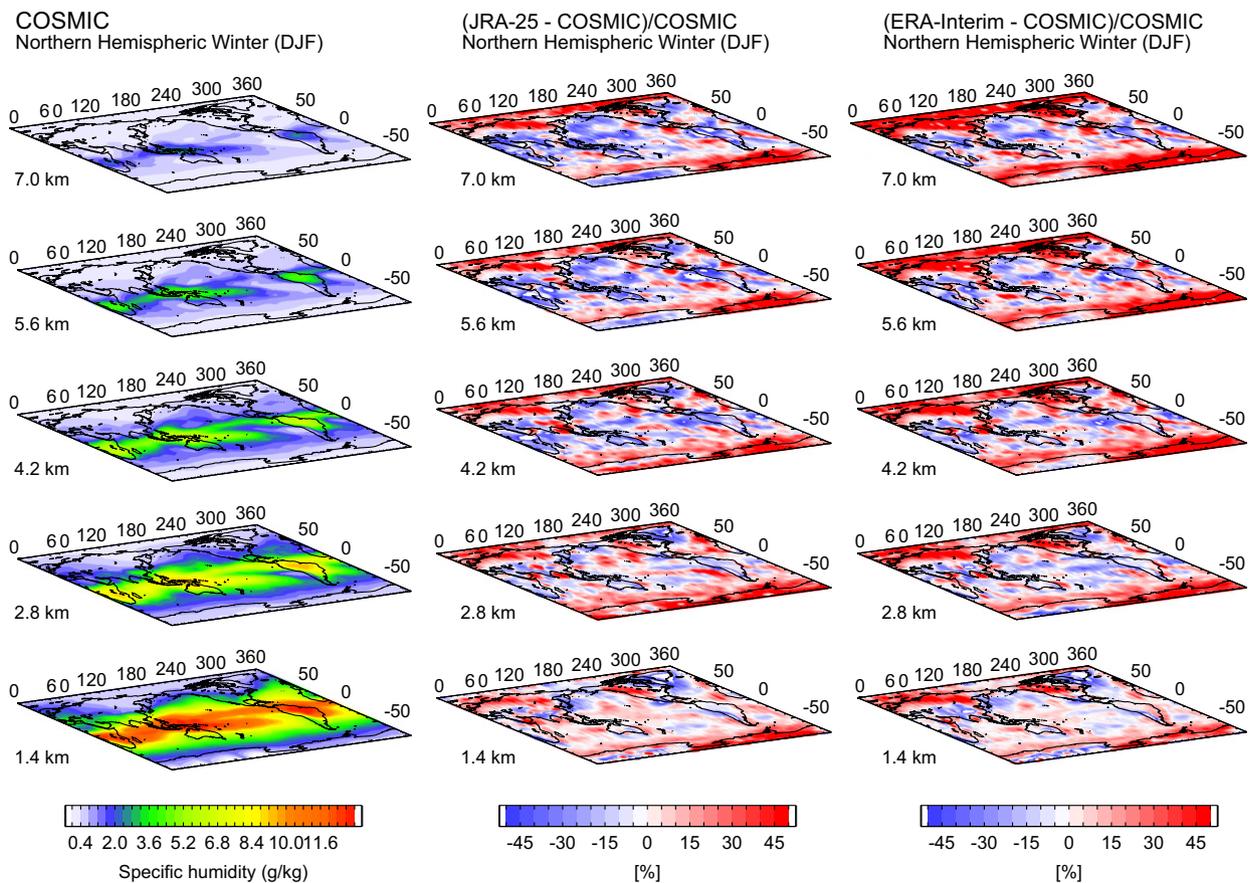

Fig. 3. Same as Fig. 2, but for the NH winter (DJF).

We describe the climatological differences of specific humidity in the lower troposphere observed between reanalysis and COSMIC and data sets. The longitude-latitude structure of the specific humidity relative differences between reanalysis and COSMIC data sets (reanalysis–COSMIC/COSMIC) at all the levels mentioned above are shown in middle and right panels of Figs. 2 and 3, for NH summer and NH winter, respectively. Examining the Fig. 2, in the tropics the COSMIC specific humidity values are higher than reanalysis values especially within regions of high humidity over convective regions Africa, Western Pacific, South America and north-eastern part of India and it extends up to Pacific Ocean. It is evident from the figure that the ERA-Interim model values and the COSMIC values compare better than the JRA-25 reanalysis data sets. Note that the red (blue) color denotes COSMIC is drier (wetter). The reanalysis values are little higher than the COSMIC at subtropics. Large difference is observed between COSMIC and ERA-Interim than COSMIC and JRA-25 in polar latitudes also COSMIC shows higher humidity than model data sets during NH summer and NH winter.

From Fig. 3 it is clear that COSMIC observations in NH winter show higher values than reanalysis in the tropics and lower specific humidity values in the subtropics at lower levels. For equatorial region, the average NH winter specific humidity is about 10–30% higher in COSMIC than the reanalysis values, in the case of subtropics the differences range from 5% to 10% and COSMIC is lower than the reanalysis values. The most significant difference between reanalysis and COSMIC data sets occur in the tropics and

the differences observed in NH summer are significantly larger than the NH winter. Kursinski and Hajj (2001) calculated latitude-altitude specific humidity differences between GPS/MET–NCEP and GPS/MET–ECMWF operational reanalysis using June and July 1995 data sets. They noted a mean specific humidity difference of 2 g/kg (~16%) in the tropical low latitude regions.

The agreement between both reanalysis and COSMIC data sets is quite good except for some specific regions where COSMIC values are higher than the reanalysis values. This overestimation of the water vapor content by COSMIC (or the underestimation by the reanalysis values) seems to occur preferably over convective regions of Africa, Western Pacific, and South America. On the other hand, problems of the reanalysis data at these regions can also not be excluded; because it is unclear how many real measurements (e.g., radiosonde data) went into the reanalysis at these locations. More detailed discussion on the differences will be dealt in Section 3.3.

The vertical cross section of zonally averaged mean specific humidity differences between the ERA-Interim, JRA-25, NCEP reanalysis, and COSMIC data averaged during 2006–2009 is shown in Fig. 4(a)–(c), respectively. It is interesting to see that in the equatorial latitude (20°S–20°N) the differences are negative above 800 mb and these negative differences extend up to 400 mb in JRA-25. The negative difference between NCEP and COSMIC starts from 900 mb. Below 800 mb the differences in tropics for ERA-Interim reanalysis and COSMIC are of the order of
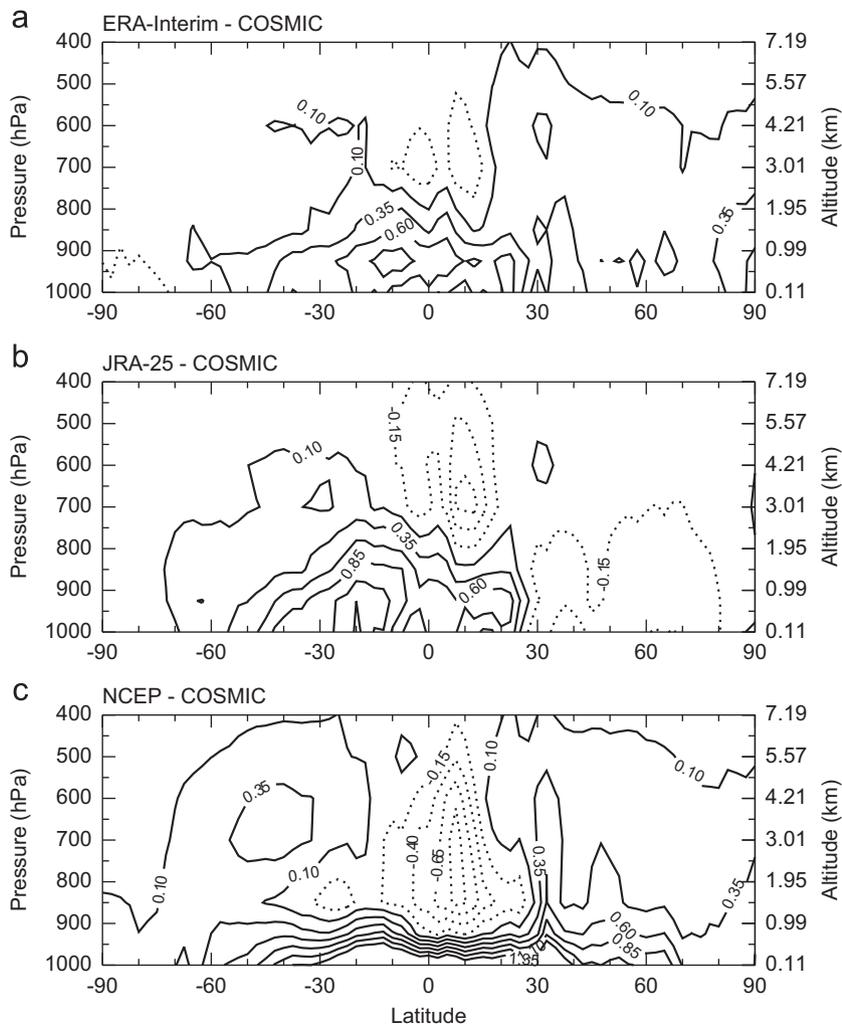

Fig. 4. Zonal mean latitudinal difference in the specific humidity (g/kg) observed between COSMIC and (a) ERA-Interim, (b) JRA-25, (c) NCEP observed during 2006–2009. The contour interval is 0.25 (g/kg).

~0.9 g/kg, and slightly less in extra-tropical latitudes (up to ~0.5 g/kg). The ERA-Interim reanalysis values are little larger at extra-tropics, Northern and Southern mid and high latitude regions. Differences are higher over the tropical regions, in particular the land regions of Africa and South America but these are much less than unity. The differences in the SH extra-tropics is slightly higher than in the NH. Pierce et al. (2006) has compared water vapor from AIRS satellite measurements with model values and found that the majority of models have a pattern of drier than observed conditions by 10–25% in the tropics below 800 hPa, but 25–100% in moist conditions between 300 and 600 hPa, especially in the extra-tropics. John and Soden (2007) showed generally good agreement between AIRS and reanalyses, where both AIRS

and reanalyses disagreed with climate models. Kursinski and Hajj (2001) reported the negative differences in specific humidity at almost all latitudes except the band between 5°S and 30°N using the GPS/MET and NCEP data sets during June and July 1995. For the tropical ocean, the reanalysis data sets are based on indirect assessment of satellite data such as outgoing long-wave radiation (OLR) and are dependent on the algorithm used to estimate the rainfall so that there is some uncertainty in these estimates.

3.3. Latitudinal variations of specific humidity

In order to examine more clearly the latitudinal variations, Fig. 5 shows the specific humidity for the NH summer and NH
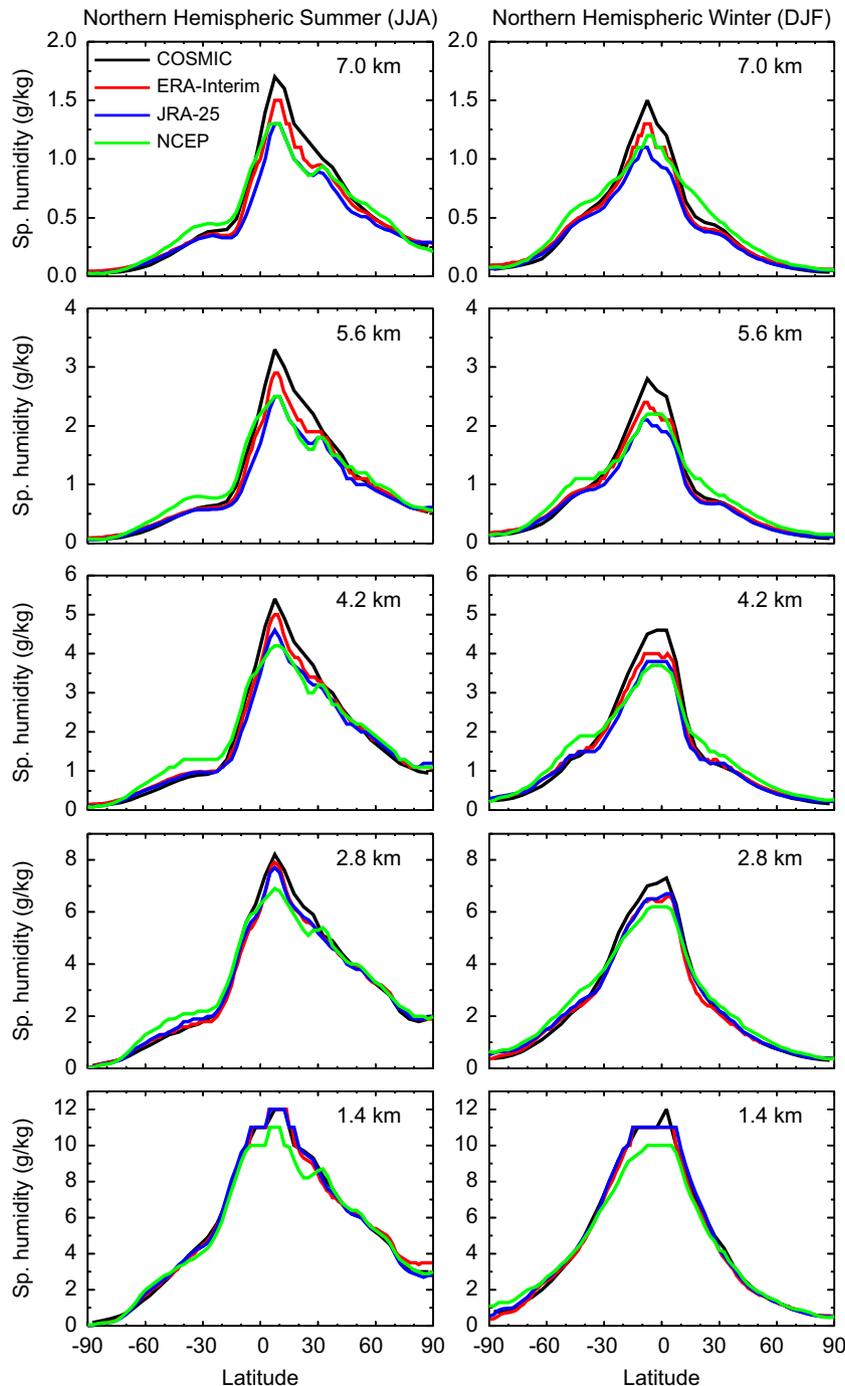

Fig. 5. Latitudinal distribution of mean specific humidity observed at different altitude levels by COSMIC, ERA-Interim, JRA-25, and NCEP during NH summer (left panels) and NH winter (right panels) seasons.

winter seasons at all the levels for COSMIC, ERA-Interim, JRA-25, and NCEP. Specific humidity shows peak values in the tropics, shifted from the equator toward the summer hemisphere, and decrease toward the pole. The mean specific humidity of NH summer (NH winter) peak centered near $5°N–10°N$ ($5°S–10°S$), the approximate location of the ITCZ, and the maximum values at about 14 g/kg are found near the ITCZ between 0.75 and 1.5 km altitude (figure not shown). Comparing the seasonal features, the NH winter values are little smaller than the NH summer values in both observations and reanalysis data sets. There is also a secondary peak near $30°S$, which appear to be associated with the transition between the subtropical zone of subsidence and the winter baroclinic region. The amplitude of COSMIC seasonal trends of specific humidity with respect to latitude resembles the same as the model outputs. On average, the COSMIC specific humidity is slightly greater than the reanalyses products at all the levels. It is interesting to see that all the data show similar values in the first level (1.4 km) in the tropics except NCEP which heavily

underestimates. The difference is increasing with increasing altitude between COSMIC and reanalysis products. It is also interesting to see that at higher levels differences between COSMIC and ERA-interim are smallest, followed by NCEP and JRA-25 reanalysis.

Difference statistics and cross correlations only provide information on the first and second moments of the distributions, so in order to look in more detail into statistics of specific humidity, we plotted the histograms and scatter diagram showing the results of NH winter specific humidity of ERA-Interim and COSMIC (Fig. 6) and JRA-25 and COSMIC (Fig. 7) at all the levels for three different latitude regions. From the figure, the ERA-Interim and COSMIC results are in reasonable agreement, and the correlation coefficients vary in the range of 0.5–0.9. The scatter plots generally show a wider deviation for larger specific humidity values than for smaller estimates. As we expect specific humidity observations to have the largest effect in the tropics, we have compared the results for the three different bands i.e., $20°N–20°S$, $20°N–50°N$,
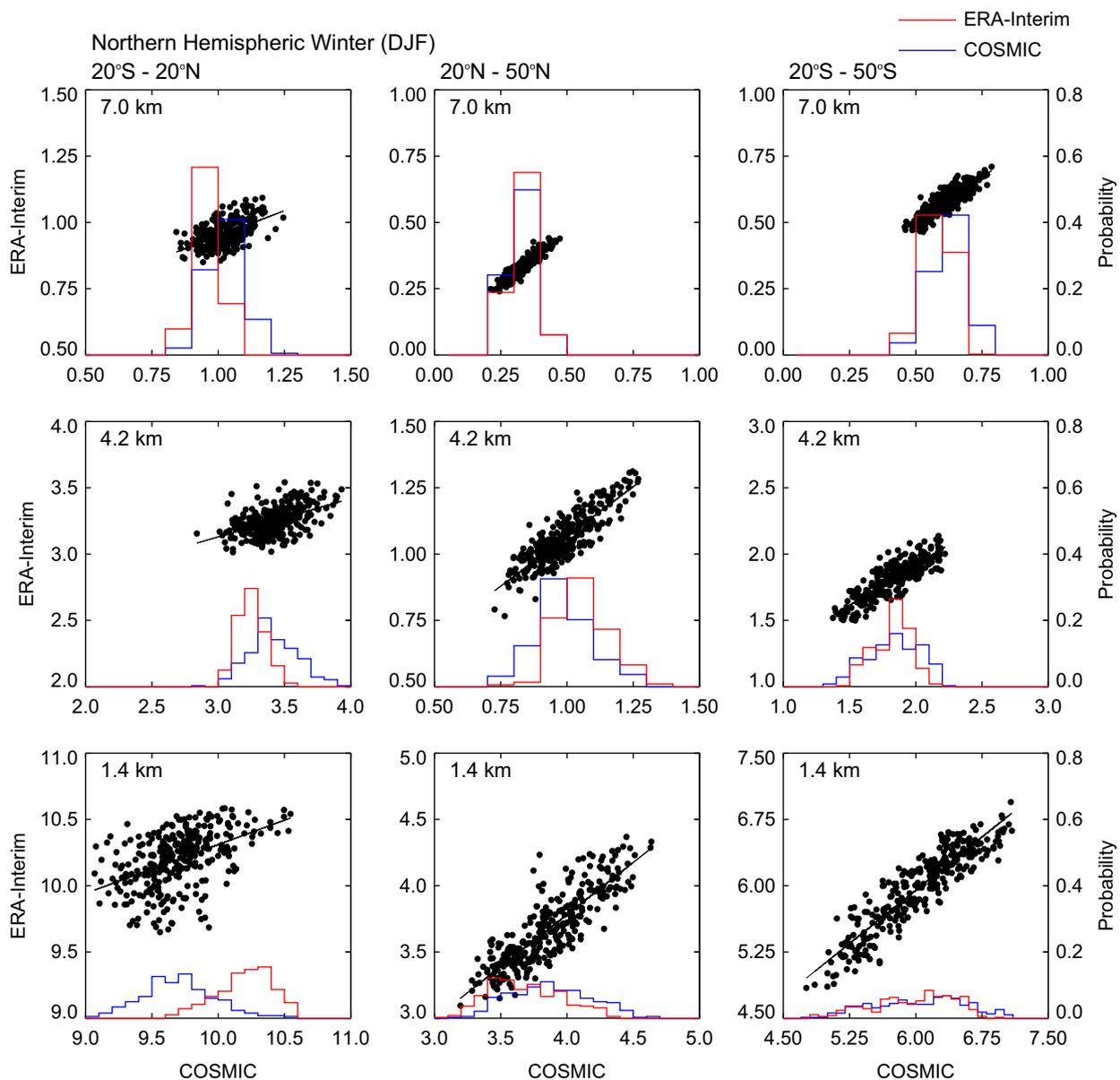
Fig. 6. Histograms showing the distributions of COSMIC and ERA-Interim reanalysis specific humidity at different altitude levels observed in latitudinal bands of 20S–20N (left panels), 20N–50N, (middle panels), and 20S–50S (right panels). Blue (red) line is for COSMIC (ERA-Interim). Dots (black line) represent the correlation (best fit) between the COSMIC and ERA-Interim reanalysis specific humidity. (For interpretation of the references to color in this figure legend, the reader is referred to the web version of this article.)

Fig. 7. Same as Fig. 6 but for COSMIC and JRA-25 data sets. Blue (red) line is for COSMIC (JRA-25). (For interpretation of the references to color in this figure legend, the reader is referred to the web version of this article.)

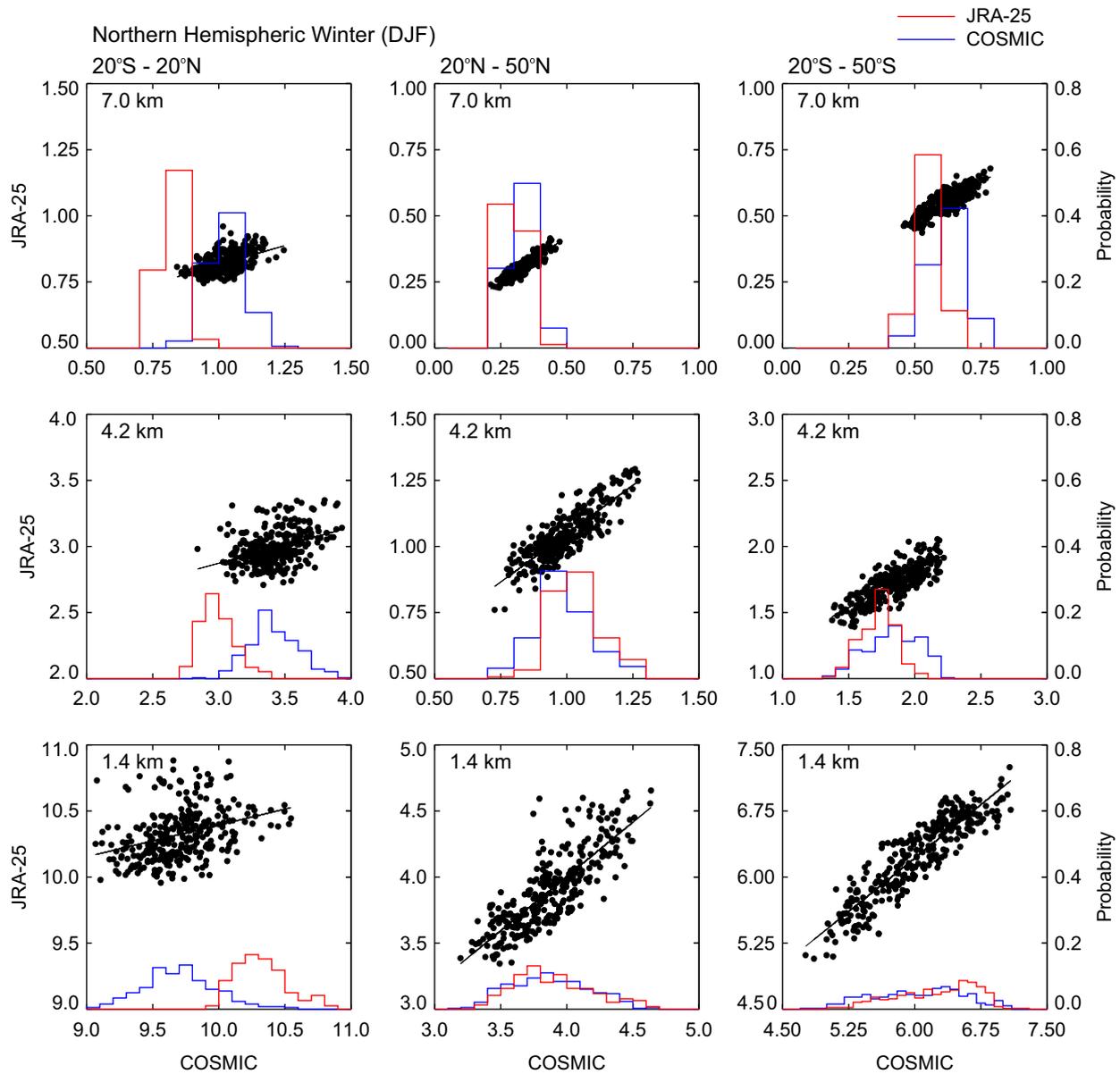and 20°S–50°S and summarized them in Table 2 for ERA-Interim and COSMIC, Table 3 for JRA-25 COSMIC, and Table 4 for NCEP reanalysis and COSMIC data sets, respectively.

From the tables, in general, the NH summer standard deviations are found higher than NH winter. In the lower troposphere, the ERA-Interim specific humidity is better than NCEP and JRA-25 reanalysis by about 10–20%. Fractional difference (ratio) is found negative in 20°N–20°S revealing that COSMIC observed values are higher than model values in both the seasons except in the first level (1.4 km) and show positive (negative) values in NH winter (NH summer) for JRA-25 and ERA-Interim. This feature is not noticed in NCEP. In addition to the performance of the models, the smaller mean difference may also be attributed to the fact that the model forecasts heavily utilize the global radiosonde measurements in the analysis. The comparison of all years NH winter and NH summer daily COSMIC and model specific humidity yields, in general, a quite low standard deviations (average 0.1–0.3 g/kg) in the 20°S–20°N latitude region. The mean differences between the model data sets and COSMIC varies within −0.2 to

0.2 g/kg. Very high correlations are observed in SH mid-latitudes followed by NH mid-latitudes with relatively poor correlations in tropical latitudes during both the seasons between reanalysis and COSMIC data sets. Correlation increases (decreases) with increase in altitude in the tropical and mid-latitudes of NH but decreases (increases) with increase in altitudes in SH mid-latitudes between ERA-Interim and JRA-25 reanalysis and COSMIC data sets during NH winter (NH summer) seasons. However, correlation increases with increase in altitude in the tropical and mid-latitudes of SH but decreases with increase in altitudes in NH mid-latitudes between NCEP and COSMIC data sets during NH summer seasons.

Histograms of the probability distribution functions (PDFs) are studied for each data set and this approach makes it possible to evaluate the consistency between data sets without the need of co-location in space and time. There are differences and similarities in the observed and modeled distributions. The 20°S–20°N peak is close to the ERA-Interim and lower than the JRA-25 reanalysis peak value. The mean value of the COSMIC in 20°S–20°N latitude band distribution is 0.13 g/kg (2.12%) greater than

Table 2
Mean specific humidity (g/kg) observed by COSMIC at various levels in different latitude bands during winter and summer seasons. Mean difference along with standard deviations observed between COSMIC and ERA-Interim data sets, ratio (=(ERA-Interim−COSMIC)/COSMIC) and correlation coefficients are also presented for different levels.

Latitude: 20S–20N (ERA-Interim–COSMIC)

	Winter (no. of points=305)				Summer (no. of points=368)			
Altitude (km)	COSMIC mean	Mean diff. ± SD	Correlation	Ratio (%)	COSMIC mean	Mean diff. ± SD	Correlation	Ratio (%)
1.4	9.70	0.50 ± 0.25	0.48	5.1	9.82	0.41 ± 0.31	0.46	4.2
2.8	5.72	− 0.15 ± 0.22	0.49	− 2.6	5.72	− 0.09 ± 0.32	0.49	− 1.6
4.2	3.42	− 0.17 ± 0.16	0.52	− 4.9	3.38	− 0.09 ± 0.22	0.49	− 2.7
5.6	1.96	− 0.14 ± 0.11	0.52	− 7.1	1.93	− 0.12 ± 0.16	0.48	− 6.4
7.0	1.02	− 0.07 ± 0.06	0.56	− 6.5	0.98	− 0.05 ± 0.09	0.33	− 5.4
Latitude: 20N–50N								
1.4	3.87	− 0.16 ± 0.16	0.85	− 4.9	7.71	− 0.08 ± 0.28	0.92	− 1.0
2.8	1.85	− 0.01 ± 0.09	0.84	1.8	4.85	− 0.06 ± 0.22	0.90	− 1.3
4.2	0.99	0.07 ± 0.06	0.86	7.1	2.95	− 0.01 ± 0.17	0.85	− 0.2
5.6	0.59	0.01 ± 0.03	0.90	1.9	1.67	− 0.04 ± 0.12	0.82	− 2.8
7.0	0.33	0.01 ± 0.02	0.92	0.6	0.85	− 0.02 ± 0.07	0.80	− 2.6
Latitude: 20S–50S								
1.4	4.19	− 0.11 ± 0.20	0.75	− 2.6	6.03	− 0.06 ± 0.21	0.91	− 0.1
2.8	1.71	0.02 ± 0.14	0.74	1.2	3.21	− 0.10 ± 0.16	0.90	− 3.1
4.2	0.88	0.07 ± 0.09	0.75	7.7	1.84	− 0.02 ± 0.11	0.85	− 0.9
5.6	0.53	0.01 ± 0.05	0.81	1.0	1.09	− 0.05 ± 0.06	0.85	− 4.7
7.0	0.28	0.01 ± 0.03	0.81	0.4	0.62	− 0.04 ± 0.03	0.87	− 5.6

Table 3
Same as Table 2 but for COSMIC and JRA-25 reanalysis data sets.

Latitude: 20S–20N (JRA-25–COSMIC)

	Winter (no. of points=305)				Summer (no. of points=368)			
Altitude (km)	JRA-25 mean	Mean diff. ± SD	Correlation	Ratio (%)	JRA-25 mean	Mean diff. ± SD	Correlation	Ratio (%)
1.4	10.32	0.62 ± 0.28	0.34	6.4	10.26	0.44 ± 0.32	0.41	4.5
2.8	5.62	− 0.10 ± 0.23	0.45	− 1.8	5.67	− 0.05 ± 0.34	0.35	− 0.9
4.2	2.99	− 0.43 ± 0.18	0.40	− 12.6	3.03	− 0.35 ± 0.26	0.30	− 10.2
5.6	1.61	− 0.35 ± 0.11	0.50	− 17.7	1.57	− 0.36 ± 0.17	0.32	− 18.7
7.0	0.82	− 0.20 ± 0.06	0.53	− 19.8	0.78	− 0.19 ± 0.10	0.29	− 19.8
Latitude: 20N–50N								
1.4	3.90	0.03 ± 0.18	0.82	0.7	7.86	0.15 ± 0.30	0.91	1.9
2.8	2.02	0.17 ± 0.10	0.83	9.1	4.87	0.02 ± 0.25	0.87	0.3
4.2	1.04	0.05 ± 0.06	0.85	5.3	2.85	− 0.10 ± 0.19	0.81	− 3.5
5.6	0.57	− 0.02 ± 0.04	0.89	− 4.1	1.50	− 0.17 ± 0.13	0.77	− 10.3
7.0	0.30	− 0.03 ± 0.02	0.91	− 7.6	0.76	− 0.09 ± 0.07	0.76	− 10.9
Latitude: 20S–50S								
1.4	4.19	0.01 ± 0.20	0.74	0.1	6.24	0.21 ± 0.22	0.91	3.5
2.8	1.89	0.18 ± 0.15	0.71	10.5	3.24	0.03 ± 0.16	0.90	1.0
4.2	0.91	0.03 ± 0.09	0.70	3.0	1.72	− 0.11 ± 0.12	0.81	1.0
5.6	0.51	− 0.02 ± 0.05	0.79	− 3.8	0.98	− 0.11 ± 0.07	0.81	− 10.0
7.0	0.27	− 0.01 ± 0.03	0.79	− 3.8	0.55	− 0.07 ± 0.04	0.83	− 10.6

ERA-Interim, −0.14 g/kg (2.28%) lesser than JRA-25, and 0.15 g/kg (2.45%) higher than NCEP reanalysis at 2.8 km for NH summer season. In the tropics, the distribution from ERA-Interim, JRA-25, and NCEP reanalysis are more strongly peaked than the COSMIC at all altitude levels. For the other two latitude bands, the shapes of the distributions from COSMIC and reanalysis are similar. The absolute mean values of models and COSMIC are differing by not more than 0.5 g/kg for any season in all the levels. A noticeable difference between the model outputs and COSMIC is that COSMIC shows less moisture in the tropical latitude (20°S–20°N) at 1.4 km altitude level.

The specific humidity in low latitudes from the ERA-Interim and JRA-25 reanalysis is in reasonable agreement with the specific humidity retrieved from the COSMIC RO observations. Both data sets show high specific humidity closely related with tropical deep convection. There is, however, clear evidence of differences/underestimate of specific humidity in the JRA-25 reanalysis, especially summer/winter seasons.

4. Conclusions

GPS radio occultations provide high-resolution vertical profiles of the atmospheric refractivity that can be used to extract vertical profiles of tropospheric moisture content. Specific humidity profiles in the lower troposphere on the basis of COSMIC RO measurements for the period of September 2006–December 2009 have been discussed. As a first step towards building the COSMIC water vapor climatology, reasonable global maps of seasonal mean of specific humidity at different pressure levels are derived

Table 4
Same as Table 2 but for COSMIC and NCEP reanalysis data sets.

Latitude: 20S–20N (NCEP–COSMIC)								
Winter (no. of points = 305)					**Summer (no. of points = 368)**			
Altitude (km)	NCEP mean	Mean diff. ± SD	Correlation	Ratio (%)	NCEP mean	Mean diff. ± SD	Correlation	Ratio (%)
1.4	9.18	−0.52 ± 0.28	0.37	−5.4	9.25	−0.57 ± 0.34	0.32	−5.8
2.8	5.36	−0.37 ± 0.26	0.38	−6.4	5.48	−0.24 ± 0.36	0.37	−4.2
4.2	3.04	−0.38 ± 0.20	0.40	−11.0	3.17	−0.21 ± 0.26	0.30	−6.1
5.6	1.80	−0.16 ± 0.13	0.43	−8.2	1.79	−0.14 ± 0.18	0.39	−7.2
7.0	0.97	−0.06 ± 0.07	0.51	−5.7	0.93	−0.05 ± 0.10	0.39	−5.3
Latitude: 20N–50N								
1.4	3.80	−0.08 ± 0.18	0.81	−1.9	7.62	−0.10 ± 0.35	0.89	−1.2
2.8	2.16	0.31 ± 0.10	0.82	16.5	4.78	−0.07 ± 0.28	0.85	−1.3
4.2	1.24	0.26 ± 0.06	0.83	26.3	2.82	−0.13 ± 0.20	0.79	−4.4
5.6	0.73	0.14 ± 0.04	0.84	23.0	1.56	−0.11 ± 0.13	0.76	−6.9
7.0	0.41	0.08 ± 0.02	0.87	25.1	0.83	−0.09 ± 0.07	0.74	−2.2
Latitude: 20S–50S								
1.4	3.94	−0.25 ± 0.22	0.66	−6.0	5.82	−0.21 ± 0.25	0.90	−3.4
2.8	2.18	0.47 ± 0.16	0.64	17.2	3.52	0.30 ± 0.19	0.87	9.5
4.2	1.25	0.37 ± 0.10	0.69	18.9	2.04	0.21 ± 0.12	0.78	11.3
5.6	0.72	0.19 ± 0.06	0.75	18.4	1.20	0.11 ± 0.07	0.81	9.9
7.0	0.38	0.09 ± 0.04	0.73	19.3	0.69	0.07 ± 0.04	0.82	11.4

and compared with ground based radiosondes and model outputs (ERA-Interim, JRA-25, and NCEP). The main conclusions drawn from the present study are summarized below.

1. Good agreement between COSMIC derived water vapor and GPS radiosondes is found up to 8 km suggesting that COSMIC derived water vapor information is reliable up to 8 km (assuming radiosonde as standard technique).
2. Majority of model outputs show wet bias compared to COSMIC by 10–25% in the tropics below 800 hPa, but dry bias of about 25–50% above 800–400 hPa. The differences in the SH extra-tropics are slightly higher than in the NH.
3. Among the model outputs, ERA-Interim show near realistic values to that observed by COSMIC followed by NCEP and JRA-25 at higher levels. NCEP heavily underestimates at lower levels.
4. Very high correlations are observed in SH mid-latitudes followed by NH mid-latitudes with relatively poor correlations in tropical latitudes during both the seasons between COSMIC and reanalysis data sets.
5. Correlation increases (decreases) with increase in altitude in the tropical and mid-latitudes of NH but decreases (increases) with increase in altitudes in SH mid-latitudes between COSMIC and ERA-Interim and JRA-25 reanalysis data sets during NH winter (summer) seasons. However, correlation increases with increase in altitude in the tropical and mid-latitudes of SH but decreases with increase in altitudes in NH mid-latitudes between COSMIC and NCEP data sets during NH summer seasons.
6. The movement of higher specific humidity band associated with ITCZ is clearly observed.
7. The zonal mean specific humidity values in the NH summer is slightly larger than NH winter.

Both satellite and reanalysis observations have their advantages and weaknesses: reanalysis values suffer from a sparse input of data and satellite measurement errors are related to atmospheric propagation effects, such as the super refraction, and may not be overcome unless applying additional constraints (Sokolovskiy, 2003a). In addition, there is evidence that elongated (layered) irregularities of refractivity with small vertical scales may result in inversion errors with significantly larger vertical scales and magnitudes up to several percent (Sokolovskiy, 2003b).

The good agreement between COSMIC and radiosonde data sets encourages the use of COSMIC measurements for describing the spatial and temporal variability of lower tropospheric specific humidity. We notice that LEO RO missions like COSMIC will provide a significantly extended database which will allow for global coverage Furthermore, RO data will be of growing interest for climatological investigations in the future when the medium and long-term RO data sets become available.

Acknowledgments

References

Angell, J.K., 2003. Effect of exclusion of anomalous tropical stations on temperature trends from a 63-station radiosonde network, and comparison with other analyses. J. Climate 16, 2288–2295.

Anna Agustı-Panareda, et al., 2009. Radiosonde humidity bias correction over the West African region for the special AMMA reanalysis at ECMWF. Q. J. R. Meteorol. Soc. 135, 595–617.

Anthes, R., Rocken, C., Kuo, Y.H., 2000. Applications of COSMIC to meteorology and climate. Terr. Atmos. Ocean. Sci. 11, 115–156.

Anthes, R.A., et al., 2008. The COSMIC/FORMOSAT-3 mission: early results. Bull. Am. Meteorol. Soc. 89, 1–21.

Ao, C.O., Meehan, T.K., Hajj, G.A., Mannucci, A.J., Beyerle, G., 2003. Lower troposphere refractivity bias in GPS occultation retrievals. J. Geophys. Res. 108 (D18), 4577. doi:10.1029/2002JD003216.

Bauer, R., Schlussel, R., 1993. Rainfall, total water, ice water and water vapor over sea from polarized microwave simulations and special sensor Microwave Imager data. J. Gephys. Res. 98 (D11), 20737–20759.

Beyerle, G., Wickert, J., Schmidt, T., Reigber, C., 2004. Atmospheric sounding by global navigation satellite system radio occultation: an analysis of the negative refractivity bias using CHAMP observations. J. Geophys. Res. 109, D01106. doi:10.1029/2003JD003922.

Dee, D.P., Uppala, S., 2009. Variational bias correction of satellite radiance data in the ERA-Interim reanalysis. Q. J. R. Meteorol. Soc.. doi:10.1002/qj.493.

Gettelman, A., Collins, W.D., Fetzer, E.J., Eldering, A., Irion, F.W., Duffy, P.B., Bala, G., 2006. Climatology of upper tropospheric relative humidity from the atmospheric Infrared sounder and implications for climate. J. Climate 19, 6104–6121.

Hajj, G.A., Kursinski, E.R., Romans, L.J., Bertiger, W.I., Leroy, S.S., 2002. A technical description of atmospheric sounding by GPS occultation. J. Atmos. Solar-Terr. Phys. 64, 451–469.

Held, I., Soden, B., 2000. Water vapor feedback and global warming. Annu. Rev. Energy Environ. 25, 441–475.

Ho, S.-P., Zhou, X., Kuo, Y.-H., Hunt, D., Wang, J.H., 2010. Global evaluation of radiosonde water vapor systematic biases using GPS radio occultation from COSMIC and ECMWF analysis. Remote Sens. 2, 1320–1330. doi:10.3390/rs2051320.

Hocke, K., 1997. Inversion of GPS meteorology data. Ann. Geo. Phys. 15, 443–450.

John, V.O., Soden, B.J., 2007. Temperature and humidity biases in global climate models and their impcat on climate feedbacks. Geophys. Res. Lett. 34, L18704. doi:10.1029/2007GL030429.

Kalnay, E., Kanamitsu, M., Kistler, R., Collins, W., Deaven, D., Gandin, L., et al., 1996. The NCEP/NCAR 40-year reanalysis project. Bull. Am. Meteor. Soc. 77, 437–471.

Kistler, R., Kalnay, E., Collins, W., Saho, S., White, G., Woolen, J., Chelliah, M., Ebisuzaki, W., Kanamitsu, M., Kousky, H., Van den Dool, Jenne, R., Fiorino, H., 2001. The NCEP-NCAR 50-year reanalysis: monthly means CD-ROM and documentation. Bull. Am. Meteor. Soc. 82, 247–267.

Kuo, Y.H., Schreiner, W.S., Wang, J., Rossister, D.L., Zhang, Y., 2005. Compariosn of GPS radio occulation soundings with radiosondes. Geophys. Res. Lett. 32, L05817. doi:10.1029/2004GL021443.

Kursinski, E.R., Hajj, G.A., Schofield, J.T., Linfield, R.P., Hardy, K.R., 1997. Observing earth's atmosphere with radio occultation measurements using the global positioning system. J. Geophys. Res. 102 (D19), 23429–23465.

Kursinski, E.R., Hajj, G.A., 2001. A comparison of water vapor derived from GPS occultations and global weather analyses. J. Geophys. Res. 106 (D1), 1113–1138.

Lanzante, J.R., Klein, S.A., 2003a. Temporal homogenization of monthly radiosonde temperature data. Part I: methodology. J. Climate 16, 224–240.

Lanzante, J.R., Klein, S.A., Seidel, D.J., 2003b. Temporal homogenization of monthly radiosonde temperature data. Part II: sensitivities, and MSU comparison. J. Climate 16, 241–262.

Luers, J.K., Eskridge, R.E., 1998. Use of radiosonde temperature data in climate studies. J. Climate 11, 1002–1019.

Melbourne, W.G., et al., 1994. The application for space borne GPS to atmospheric limb sounding and global change monitoring. Jet Propul. Lab. Rep. 94 (18) (147 pp).

Onogi, K., Tsutsui, J., Koide, H., Sakamoto, H., Kobayashi, S., Hatsushika, H., Matsumoto, T., Yamazaki, N., Kamahori, H., Takahashi, K., Kadokura, S., Wada, K., Kato, K., Oyama, R., Ose, T., Mannoji, N., Taira, R., 2007. The JRA-25 reanalysis. J. Meteor. Soc. Jpn. 85, 369–432.

Oort, A.H., 1983. Global atmospheric circulation statistics, 1958–1973. NOAA Prof. Paper 14, 180 pp. and microfiche (available from author at GFDL/NOAA, P.O. Box 308, Princeton, NJ, 08542).

Peixoto, J.P., Oort, A.H., 1996. The climatology of relative humidity in the atmosphere. J. Climate 9, 3443–3463.

Pierce, D.W., Barnett, T.P., Fetzer, E.J., Gleckler, P.J., 2006. Three-dimentional tropospheric water vapor in coupled climate models compared with observations from the AIRS satellite system. Geophys. Res. Lett. 33, L21701. doi:10.1029/2006GL027060.

Poli, P., Joiner, J., Kursinski, E.R., 2002. 1DVAR analysis of temperature and humidity using GPS radio occultation refractivity data. J. Geophys. Res. 107 (D20), 4448. doi:10.1029/2001JD000935.

Prabhakara, C., Chang, H.D., Chang, A.T.C., 1982. Remote sensing of precipitable water over the oceans from Nimbus 7 microwave measurements. J. Appl. Meteor. 21, 59–68.

Ramanathan, V., 1981. The role of ocean-atmospheric interactions in the CO_2 climate problem. J. Atmos. Sci. 38, 918–930.

Rao, D.N., Venkat Ratnam, M., Mehta, Sanjay, Nath, Debashis, Basha, Ghouse, Jagannadha Rao, V.V.M., Krishna Murthy, B.V., Tsuda, T., Nakamura, Kenji, 2009. Validation of the COSMIC radio occultation data over gadanki (13.48oN, 79.2oE): a tropical region. Terr. Atmos. Ocean. Sci. 20, 59–70. doi:10.3319/TAO.2008.01.23.01(F3C).

Randel, W.J., Wu, F., 2006. Biases in stratospheric and tropospheric temperature trends derived from historical radiosonde data. J. Climate 19, 2094–2104.

Rocken, C., Anthes, R., Exner, M., Hunt, D., et al., 1997. Analysis and validation of GPS/MET data in the neutral atmosphere. J. Geophys. Res. 102 (D25), 29 849–29 866.

Rosenlof, K.H., Reid, G.C., 2008. Trends in the temperature and water vapor content of the tropical lower stratosphere: sea surface connection. Geophys. Res. Lett. 113, D06107. doi:10.1029/2007JD009109.

Ross, R.J., Elliott, W.P., 1996. Tropopsheric water vapour climatology and trends over North America: 1973–93. J. Climate 9, 3561–3574.

Schreiner, W., Rocken, C., Sokolovskiy, S., Syndergaard, S., Hunt, D., 2007. Estimates of the precision of GPS radio occultations from the COSMIC/FORMOSAT-3 mission. Geophys. Res. Lett. 34, L04808. doi:10.1029/2006GL027557.

Simmons, A.J., Hollingsworth, A., 2002. Some aspects of the improvement in skill of numerical prediction. Q. J. R. Meteorol. Soc. 128, 647–677.

Simmons, A.J., Hortal, M., Kelly, G., McNally, A., Untach, A., Uppala, S., 2005. ECMWF analyses and forecasts of stratospheric winter polar vortex breakup: September 2002 in the southern hemisphere and related events. J. Atmos. Sci. 62, 668–689.

Simmons, A.J., Uppala, S., Dee, D.P., 2007b. Update on ERA-Interim. ECMWF Newslett. 111, 5.

Seidel, D.J., Coauthors, 2004. Uncertainty in signals of large scale climate variations in radiosonde and satellite upper-air temperature data sets. J. Climate 17, 2225–2240.

Soden, B.J., Turner, D.D., Lesht, B.M., Miloshevich, L.M., 2004. An analysis of satellite, radiosonde, and lidar observations of upper tropospheric water vapor from the Atmospheric Radiation Measurement Program. J. Geophys. Res. 109, D04105. doi:10.1029/2003JD003828.

Sokolovskiy, S., 2003a. Effect of super refraction on inversions of radio occultation signals in the lower troposphere. Radio Sci. 38, 1058. doi:10.1029/2002RS002728.

Sokolovskiy, S., 2003b. Effect of super refraction and small-scale refractivity irregularities on inversion of radio occultation signals in the lower troposphere. In: Proceedings of the International Workshop on GPS Meteorology, Tsukuba, Japan, MEXT and JISTEC, pp. 2071–2075.

Sokolovskiy, S., Rocken, C., Hunt, D., Schreiner, W., Johnson, J., Masters, D., Esterhuizen, S., 2006. GPS profiling of the lower troposphere from space: inversion and demodulation of the open-loop radio occultations signals. Geophys. Res. Lett. 33, L14816. doi:10.1029/2006GL026112.

Trenberth, K.E., Guillemot, C.J., 1995. Evaluation of the global atmospheric moisture budget as seen from analyses. J. Climate 8, 2255–2272.

Uppala, S.M., Dee, D.P., Kobayashi, S., Berrisford, P., Simmons, A.J., 2008. Towards a climate data assimilation system: status update of ERA-Interim. ECMWF Newslett. 115, 12–18.

Wang, J., Carlson, D.J., Parsons, D.B., Hock, T.F., Lauritse, D., Cole, H.L., Beierle, K., Chamberlain, E., 2003. Performance of operational radiosonde humidity sensors in direct comparison with a chilled mirror dew-point hygrometer and its climate implication. Geophys. Res. Lett. 30 (16), 1860. doi:10.1029/2003GL016985.

Wickert, J., Reigber, C., Beyerle, G., Konig, R., Marquardt, C., co authors, 2001. Atmosphere sounding by GPS radio occultation: first results from CHAMP. Geophys. Res. Lett. 28 (17), 3263–3266.

Wickert, J., Schmidt, T., Beyerle, G., Konig, R., Reigber, C., 2004. The radio occultation experiment aboard CHAMP: operational data analysis and validation of vertical atmospheric profiles. J. Met. Soc. Jpn. 82, 381–395.